Supplementary material

A novel adeno-associated virus capsid with enhanced neurotropism enables correction of a lysosomal transmembrane enzyme deficiency

Supplementary Methods

Recombinant AAV vector production

Recombinant AAV virions were produced by transient transfection of HEK 293T cells using polyethylenimine (PEImax, Polysciences Inc.) with two plasmids: one plasmid encoding the transgene cassette flanked by ITRs of AAV2 (AAV-CAG-coHGSNAT or pTRUF-11 (ATCC, MBA-331)) and the pDG plasmid expressing AAV2 Rep and either the AAV2, AAV9, AAV-rh10 or AAV-TT Cap gene, and adenovirus 5 helper functions necessary for virion formation (Grimm, 1998). Cells were harvested 72 hours post transfection; crude cell lysate was produced by repeated freeze/thawing of the cell pellets in lysis buffer to release the virus. In parallel, the virus-containing supernatant was harvested and precipitated using ammonium sulphate salt. The cell lysate and precipitated supernatant were treated with benzonase to digest cellular and non-encapsidated DNA, clarified by centrifugation and filtered at 0.22µm before purification.

AAV-TT, AAV2 and AAV-rh10 virus preparations were purified using the AKTApurifier chromatography system (GE Healthcare) and an AVB sepharose affinity column (buffer A: PBS, pH 8; buffer B: 0.5M glycine, pH 2.7). The AAV9 vector was purified by iodixanol step gradient: the viral preparation was overlaid with increasing concentrations (15%, 25%, 40% and 60%) of iodixanol (OptiPrep; Sigma). The tubes were centrifuged at 40,000 rpm for 3 hours at 18˚C in a Sorvall Discovery 90SE ultracentrifuge using a TH641 rotor (Thermo Scientific). The vector was extracted from the 40% fraction with a 19-gauge needle. Purified vector fractions were dialysed against PBS overnight.

We performed real time PCR and alkaline gel electrophoresis to assess the viral genome titers and integrity of the viral genome (Zeltner, 2010; Fagone, 2012), the capsid titers were determined by SDS PAGE electrophoresis (Kohlbrenner, 2012).

Intraocular injections

Intraocular injections were performed under general anaesthesia using an operating microscope. 6-week old mice were anaesthetised by intraperitoneal injection using a mixture of medetomidine hydrochloride (1mg/mL, Domitor, Pfizer Pharmaceuticals), ketamine (100mg/mL, Fort Dodge Animal Health) and sterile water in the ratio 5:3:42. Viral vectors were injected at a dose of 2 x 10^9 vg per eye and each mouse received an injection of AAV-TT in one eye and an injection of AAV2 in the contra-lateral eye. 2µL of vector was delivered per injection. The eye to be injected was dilated by topical application of tropicamide 1% (Chauvin Pharmaceuticals). Corneal refractive power was neutralised by placing a 5mm coverslip on the cornea covered with a coupling medium solution (Viscotears, Novartis Pharmaceuticals) and the fundus brought into focus. The eye was secured in position by grasping the conjunctiva using corneal notched forceps (Acrofine). A 10mm, 34-gauge needle was used for vector injection. For the sub-retinal route, the tip of the needle was placed underneath the cover slip and penetrated the eye tangentially through the sclera below the equator of the globe into the subretinal space. For intravitreal injections, the tip of the needle was placed underneath the cover slip and penetrated the eye tangentially through the sclera just below the limbus and above the edge of peripheral retina. Material was then injected and the needle withdrawn. After injection, 1% chloramphenicol ointment (FDC International) was applied topically on the cornea and anaesthesia was reversed with 0.2mL of intraperitoneal atipamezole hydrochloride (0.10mg/mL, Antisedan, Pfizer Pharmaceuticals).

Immunohistochemical staining

For GFP immunohistochemical staining of neonatal mouse brain sections, endogenous peroxidase activity was depleted by incubating sections in 1% H_2O_2 in tris-buffered saline (TBS) for 30 minutes and washed (x3) in TBS. Endogenous non-specific protein binding was blocked by incubation in 15% normal serum (Sigma) in TBS-T (TBS with 0.3% Triton X-100) for 30

minutes. Sections were incubated overnight in 10% normal serum in TBS-T with primary antibody for GFP (1:4,000, ab290, Abcam). Following washes in TBS, sections were incubated in 10% normal serum in TBS-T with biotinylated secondary antibody goat anti-rabbit IgG (1:1,000, BA-1000, Vector Laboratories) for 2 hours. Staining was visualised using Vectastain avidin–biotin solution (ABC, Vector Labs) and DAB (Sigma), after which the sections were mounted, dehydrated and coverslipped with DPX (VWR). Representative images were captured using a live video camera (Nikon, DS-Fil) mounted onto a Nikon Eclipse E600 microscope.

For immunohistochemical analysis in adult rat brains, tissue sections were washed with TBS and incubated for one hour in 3% H_2O_2 in 0.5% TBS Triton solution to quench endogenous peroxidase activity. Following another washing step, the sections were blocked in 5% bovine serum for one hour and incubated with primary monoclonal antibodies overnight. Chicken anti-GFP primary antibody was used (1:20,000, ab13970, Abcam). Following overnight incubation, the primary antibody was washed away using TBS and sections were incubated for two hours with biotinylated anti-chicken secondary antibody (1:250, BA-9010, Vector Laboratories). For DAB immunohistochemistry, the ABC-kit (Vectorlabs) was used to amplify the staining intensity through streptavidin-peroxidase conjugation and followed by a DAB in 0.01% H_2O_2 reaction.

Indirect enzyme-linked immunosorbent assay (ELISA) detection of anti-AAV IgG antibodies

Total IgG antibody responses against AAV capsid proteins were measured with an ELISA assay. The AAV vectors of either serotype was diluted in coating buffer (0.1M NaHCO3, pH8.5) at 2 x 10^9 vg/ml. 50 µL of the diluted virus was loaded to each well of the 96 well ELISA plates and incubated overnight at 4°C. The plate was washed with wash buffer (PBS, 0.1% Tween). Non-specific binding was blocked with blocking buffer (1% bovine serum albumin (BSA) 0.02M Tris/HCl, 025M NaCl, pH 7.0) for 1 hour at room temperature. Eight 2-fold serial dilutions were prepared with dilution buffer (PBS, 0.05% Tween, 0.01% BSA) for each brain sample with a starting protein concentration of 10µg. 50µL of each brain homogenate dilution was applied to the plate in duplicate and incubated for 1 hour at room temperature. After washing, 100µL of 5µg/ml biotinylated goat anti-mouse IgG antibody (Vector) in dilution buffer was added to each well and incubated at room temperature for 1 hour, aspirated and washed. Each well was

incubated with 100µL of Vectastain ABC kit (Vector) for 30 minutes at room temperature and washed. 100µL of TMB substrate was loaded to each well and incubated for exactly 3 minutes at room temperature. The reaction was stopped by adding 50µL of 2.5M H_2SO_4 to each well. Light absorbance was read at 450nm to determine the maximum absorbance and at 570nm to correct for measurement errors on a Synergy HT microplate spectrophotometer (Biotek) with Gen5 software.

HGSNAT activity assay

HGSNAT activity was measured using the HGSNAT activity assay using 4-methylumbelliferyl-β-D-N-glucosaminide (MU-βGlcNH2, Moscerdam, The Netherlands) as a substrate in duplicates in a black 96-well plate. The assay was performed according to manufacturer's instructions, and control wells contained 10µL H2O, 10µL substrate and 10µL acetyl co-enzyme A whilst sample wells contained 10µL sample, 10µl substrate and 10µL acetyl co-enzyme A. The 96-well plate was covered by a plastic seal and incubated for 18 hours at 37°C. 200µL carbonate buffer pH 9.5 was added to each well to terminate the reaction. 4-MU standards (21.33µM - 0.17µM) were added to the plate, and the plate was read for fluorescence at excitation 260nm and emission 450nm. Activity was reported as µM 4-MU generated/mg protein/18 hours.

Vector copy number determination

Analysis of vector biodistribution was performed by quantitative PCR (qPCR). Genomic DNA from tissue homogenate was extracted using Qiagen DNeasy Blood and Tissue Kit. For quantification of AAV vector copy numbers, a standard curve was prepared by adding specific amounts of linearised AAV-coHGSNAT plasmid and compared against GAPDH using naïve genomic murine DNA. The primer sequences used were 5'-GGGTCATTAGTTCATAGCCCATA-3' and 3'-GCCAAGTAGGAAAGTCCCATAA-5'. SYBR Green amplifications were performed using the PowerUp SYBR Green master mix (Thermo Fisher Scientific) to a final volume of 25µL, including 5µL of DNA. Plasmid amounts were calculated to give the numbers of double-stranded vector genomes per diploid genomic equivalent.

Transduction assay

The following cell lines were used: HeLa (cervical carcinoma-derived cells), HEK293T (human embryonic kidney cells), HepG2 (liver carcinoma derived cells), C2C12 (mouse myoblast cell line), THP-1 (human monocyte cell line), Jurkat (human T lymphocyte cells) and SH-SY5Y (human neuroblast cell line). Cells were seeded a day before transduction in a 12-well plate at a density of 1.5 x 10^5 cells per well in complete media supplemented with 10% foetal bovine serum. The day of transduction, the media was removed from the cells and replaced by serum-free medium containing AAV2 or AAV-TT GFP marker viruses in a total volume of 0.5 mL, to infect cells at a MOI of 10^5 viral genomes per cell. The cells were incubated with transduction media for two hours at 37°C, rocking the plate evenly every 15 minutes. Two hours after transduction, 0.5mL of complete medium containing 10% FBS was added to each well. The cells were further incubated for 72 hours before harvesting, and flow cytometry was performed to determine the number of GFP positive cells (BD FACSCanto II, BD Biosciences).

Heparin competition assay

SH-SY5Y neuroblastoma cells (ATCC, CRL-2266) were seeded at a density of 40,000 cells per well in a 48-well plate one day before transduction. One day later, AAV2 or AAV-TT vectors encoding GFP were incubated for 30 minutes at 37°C in the presence of increasing quantities of heparin (31.25 to 500 pg of heparin per viral particle). The medium was removed from the cells and replaced by the virus/heparin mixes in a total volume of 0.2mL of serum-free media. For transduction efficiency purposes the AAV2/heparin was used at a constant MOI of 1.000 viral genomes/cell and the AAV-TT/heparin was used at an MOI of 100.000 viral genomes/cell. Two hours after transduction, 0.2mL of complete medium (DMEM/F12 +10% FBS) was added to each well. The cells were incubated for 72 hours before harvesting; flow cytometry was used to determine the number of GFP positive cells.

Production and purification of AAV-TT and AAV2 VLPs

AAV-TT capsid sequences were synthesised and cloned into the transfer vector pFastbac by GeneArt (Thermo Fisher Scientific). The transfer vector was used to generate the bacmid containing the AAV-TT VP genes by homologous recombination in DH10 cells. The recombinant bacmid was used to generate AAV-TT virus-like particles (VLPs) in *Spodoptera Frugiperda* 9 *(Sf9)* cells by the Bac-to-Bac expression system (Invitrogen) according to the manufacturer's protocol. A baculovirus expressing AAV2 VLPs was generously donated by Sergei Zolotukhin (Department of Pediatrics, University of Florida). The infected *Sf9* cells expressing AAV-TT and AAV2 VLPs were harvested by centrifugation at 15,000 rpm for 20 minutes in a JA10 rotor 72 hours post infection to generate a cell pellet and supernatant. The VLPs in the cell pellet were released by three cycles of freeze/thaws in an ethanol/dry ice slurry and a 37ºC water bath, and the sample treated with Benzonase (Millipore) at 37ºC for 1 hour after the second freeze/thaw. The virus in the supernatant was collected by centrifugation at 10,000 rpm for 20 minutes in a JA20 rotor. The VLPs in the supernatant were precipitated by 10% PEG 8000 and the virus pelleted by centrifugation at 10,000 rpm for 90 minutes in a JA20 rotor.

The clarified supernatant (from the cell pellet) and the resuspended PEG pellet was further purified by a discontinuous step iodixanol gradient and ion exchange chromatography, according to previous established protocol (Zolotukhin, 2002). In brief, the supernatant was loaded onto a step gradient composed of 4ml 60%, 4ml 40%, 5ml 25% and 7mL 15% iodixanol. The 40/25% and 25% fractions were collected by fractionation and diluted 10x with Buffer A (20mM Tris pH 8.5 and 15mM NaCl). The diluted samples were loaded onto a 5mL Q column (GE Health Care). The purified VLPs were eluted with a continuous gradient of Buffer A and Buffer B (20mM Tris pH 8.5 and 500mM NaCl) for 5 column volumes. The VLP-containing fractions were collected and concentrated for further analysis.

The purity of the AAV2 and AAV-TT VLPs was monitored by Coommassie stained SDS PAGE. To determine capsid integrity, 5µL of purified sample was loaded on carbon coated copper electron microscope (EM) grids for 2 minutes, blotted, and then stained with 2% Uranyl acetate. The grids were examined on an FEI Spirit Transmission EM. The images were collected at 46,000x magnification, and 120kV with a Gatan 2Kx2K CCD camera.

Heparin binding assay

AAV-TT and AAV2 VLPs at 100ng in PBS-MK buffer (1xPBS with 1mM $MgCl_2$, and 2.5mM KCl) were loaded onto an equilibrated 300µL heparin column (Sigma, cat # H6508) and the flow through collected by gravity flow. The column was washed with 5 column volumes of PBS-MK buffer and bound virus was eluted with increasing concentration of NaCl in PBS-MK buffer in 50mM increments. The load, wash, and elution fractions were boiled at 100^{o}C for 10 minutes and analyzed by dot blot. The samples were loaded on a nitrocellulose membrane and immunoblotted with primary antibody B1 (American Research Product), which recognises a linear epitope at the C-terminus of the AAV VP, and anti-mouse monoclonal secondary antibody (Boye, 2016).

Determination of AAV-TT and AAV2 stability

Differential Scanning Fluorimetry (DSF) was used to measure the binding of SYPRO orange dye to hydrophobic regions of AAV capsids that become exposed during unfolding. 22.5µL of either AAV-TT or AAV2 VLPs at a concentration of 0.1mg/mL in citrate phosphate buffer [$CiPO_4$ (0.2M Na_2HPO_4, and 0.1M Citric acid pH7.4)] and 2.5µl of 1%-SYPRO-Orange dye (Invitrogen Inc.) was added to each mixture to make a total reaction volume of 25µL (Rayaprolu, 2013; Rayaprolu, 2014). The assays were run in a Bio-Rad MyiQ2 Thermocycler instrument with temperature ranging from 30 to 99ºC and ramping at 0.5°C per step. The rate of change of fluorescence with temperature was recorded and the thermal profile is output as –dRFU/dT versus temperature. The thermal profile was then inverted by multiplying with -1. The peak value recorded on the thermogram is the $T_{m.}$

Supplementary figures

Supplementary Figure 1. Differential Scanning fluorimetry shows increased thermal stability of AAV-TT. (**a**) Coommassie stained SDS PAGE (left panel) and negative stained electron micrographs of AAV2 and AAV-TT particles are shown (right panel). Scale bars: 100nm. (**b**) Comparative thermal profiles of AAV2 (blue) and AAV-TT (orange) at pH 7.5 show that the AAV-TT capsid is more stable than the AAV2 capsid. The inverted measured rate of change of fluorescence with time, dRFU/dT, is shown plotted in the y axis against temperature (°C) on the x axis. The melting temperatures (Tms) are 65.5 ± 0.9ºC and 72.6 ± 0.3ºC, respectively.

Supplementary Figure 2. AAV-TT exhibits reduced in vitro transduction efficiency and lacks heparin-binding ability. (**a**) Various cells lines were transduced at a multiplicity of infection (MOI) of 10^5 viral genomes per cell; transduction efficiency of AAV-TT relative to AAV2 is shown. AAV-TT displayed different transduction efficiencies in the cell lines tested: HeLa (cervical carcinoma derived cells, n=3), 293T (human embryonic kidney cells, n=3), HepG2 (liver carcinoma derived cells, n=3), C2C12 (mouse myoblast cell line, n=2), ThP1 (human monocytic cell line, n=3), Jurkat (human T lymphocyte cells, n=3) and SH-SY5Y (human neuroblast cell line, n=2). One-way ANOVA. Data are presented as mean ± s.e.m; $p<0.0001$. (**b**) Heparin competition assay showing transduction efficiency of AAV-TT and AAV2 in SH-SY5Y neuronal cells in the presence of increasing amounts of heparin. AAV-TT transduction is not affected by the presence of heparin, confirming the loss of heparin binding ability of AAV-TT. Two-way ANOVA followed by Sidak's post-hoc multiple comparisons test. Data are presented as mean ± s.e.m; *$p < 0.05$; **$p < 0.01$; ***$p < 0.001$. (n=3 per group). (c) Column-based heparin binding assay used to assess heparin binding ability of different AAV virus like particles (VLPs). The denatured immunoblot of the column load (L), flow through (FT), wash (W) and elution fractions of AAV2 VLPs (positive control), AAV-TT VLPs (test sample), and AAV5 VLPs (negative control) shows that the heparin binding ability of AAV-TT has been abolished by the mutations at residues 585 and 588.

Supplementary Figure 3. Nigral injections in adult rats show superior transduction ability and vector spread. $3.5x10^9$ vg of GFP-expressing AAV-TT or AAV2 were injected into the substantia nigra of adult rat brains (n=3). (**a**) Representative images of brain sections show that at 4 weeks post injection, transduction levels and vector spread obtained with the AAV-TT vector were higher than those obtained with the AAV2 vector. (**b**) Representative high magnification images of GFP signal in the areas indicated on top of the images. Scale bar: 100µm.

Supplementary Figure 4. Absence of GFP expression in GFAP+ astrocytes and Iba1+ microglia/macrophages in AAV-TT-treated adult mice. Representative confocal images showing GFP expression in the thalamus of wt mice injected with AAV-TT-CAG-GFP. (**a**) GFP expression in GFAP stained brain sections. (**b**) GFP expression in lba1 stained brain sections. Scale bar: 50µm. GFP expression is exclusively found in neurons and no GFP co-localisation is observed in GFAP+ astrocytes or Iba1+ microglia.

Supplementary Figure 5. Determination of HGSNAT activity *in vitro* and *in vivo* after short-term treatment. (**a**) Treatment scheme. MPSIIIC mice received intrastriatal administration of AAV9-coHGSNAT, AAVTT-coHGSNAT or AAV-rh10-coHGSNAT and were sacrificed after 3 weeks. (**b**) HGSNAT activity measured in supernatant and lysates of 293T cells transfected with plasmid encoding coHGSNAT. Enzyme activity can only be detected in cell lysates (n=4) but not in the media (n=3) of coHGSNAT treated cells. No enzyme activity was detected in cell lysates (n=4) or in the media (n=3) of GFP transfected cells, or in the in cell lysates (n=4) and the media (n=3) of non-treated cells. (**c**) Determination of enzyme activity in brain sections R1-R5 of wt, MPSIIIC mice and AAV9-coHGSNAT, AAV-TT-coHGSNAT or AAV-rh10-coHGSNAT treated mice 1 week post injection; wt (n=3), untreated MPSIIIC (n=4), AAV9 (n=4), AAV-TT (n=4) and AAV-rh10 (n=4) treated MPSIIIC mice. (**d**) Determination of enzyme activity in brain sections R1-R5 of wt, MPSIIIC mice and AAV9-coHGSNAT, AAV-TT-coHGSNAT or AAV-rh10-coHGSNAT treated mice 3 weeks post injection; wt (n=4), untreated MPSIIIC (n=3), AAV9 (n=4), AAV-TT (n=4) and AAV-rh10 (n=4) treated MPSIIIC mice. ANOVA followed by Tukey's post-hoc multiple comparison test. Data are presented as mean ± s.e.m; *$p < 0.05$; **$p < 0.01$; ***$p < 0.001$.

Supplementary Figure 6. Little to no off-target transduction of AAV-TT in peripheral organs. Vector copy number (vg/cell) in (**a**) liver of wt (n=1), untreated MPSIIIC (n=1), AAV9 (n=6), AAV-TT (n=5) treated mice; (**c**) kidney in wt (n=1), untreated MPSIIIC (n=1), AAV9 (n=4), AAV-TT (n=5) treated mice; (**e**) spleen in wt (n=1), untreated MPSIIIC (n=1), AAV9 (n=5), AAV-TT (n=5) treated mice and (**g**) lungs in wt (n=1), untreated MPSIIIC (n=1), AAV9 (n=5), AAV-TT (n=5) treated mice. Enzyme activity in (**b**) liver in wt (n=7), untreated MPSIIIC (n=5), AAV9 (n=7), AAV-TT (n=5) treated mice; (**d**) kidney in wt (n=7), untreated MPSIIIC (n=6), AAV9 (n=7), AAV-TT (n=5) treated mice; (**f**) spleen in wt (n=7), untreated MPSIIIC (n=6), AAV9 (n=7), AAV-TT (n=5) treated mice and (**h**) lungs in wt (n=7), untreated MPSIIIC (n=6), AAV9 (n=7), AAV-TT (n=5) treated mice. ANOVA followed by Tukey's post-hoc multiple comparison test. Data are presented as mean ± s.e.m; *$p < 0.05$; **$p < 0.01$; ***$p < 0.001$

Supplementary Figure 7. AAV-TT and AAV9 correct secondary storage of GM2 and GM3 gangliosides in specific brain regions. GM2 and GM3 accumulation is reduced in the specific brain areas of AAV-coHGSNAT treated MPSIIIC mice as compared to untreated mice. (**a**) Treatment of MPSIIIC mice with both AAV9-coHGSNAT and AAV TT-coHGSNAT vectors leads to a decrease in the accumulation of GM2 in the field CA3 of the hippocampus, as compared with untreated animals. (**b**) GM3 ganglioside was significantly reduced in Medial Entorhinal cortex (MEnt) of mice treated with both AAV9-coHGSNAT and AAVTT-coHGSNAT. Scale bar: 20µm. (**c**) Representative images of G_{M2} ganglioside levels in wt, MPSIIIC, AAV9-coHGSNAT and AAV-TT-coHGSNAT treated mice. As the site of injection was 2mm lateral to the bregma the images were acquired in the saggital sections 2.04mm and two other sections equidistant to the site of injection, 1.08mm and at 3.00mm lateral from bregma as indicated in the picture using Slide Scanner Axio Scan.Z1 from Zeiss (objective 10x/0.45). Scale bar: 500µm.

Supplementary Figure 8. AAV-TT and AAV9 reduce astrocytosis. Quantification of GFAP fluorescence and representative images of GFAP, DAPI staining of wt (n=4), untreated MPSIIIC (n=3), AAV9 (n=4) and AAV-TT (n=4) treated MPSIIIC mice in the (**a**) external capsule, (**b**) caudate putamen, (**c**) amygdala and (**d**) cortex. Representative images are shown following staining of 3-4 mice per group. ANOVA followed by Tukey's post-hoc multiple comparison test. Data are mean ± s.e.m; *p < 0.05; **p < 0.01. Scale bar: 50µm.

Supplementary Figure 9. AAV-TT and AAV9 reduce LAMP2 lysososmal burden. Quantification of LAMP2 fluorescence and representative images of LAMP2/ NeuN staining of wt (n=4), untreated MPSIIIC (n=3), AAV9 (n=4) and AAV-TT (n=4) treated MPSIIIC mice in the (**a**) external capsule, (**b**) thalamus, (**c**) amygdala and (**d**) cortex. Representative images are shown following staining of 3-4 mice per group. ANOVA followed by Tukey's post-hoc multiple comparison test. Data are mean ± s.e.m; *p < 0.05; **p < 0.01. Scale bar: 50µm.

Supplementary Figure 10. AAV-TT corrects neuroinflammation over AAV9. Quantification and representative images of ILB4 staining of wt (n=4), untreated MPSIIIC (n=4), AAV9 (n=4) and AAV-TT (n=4) treated MPSIIIC mice in the (**a**) hippocampus, (**b**) thalamus, (**c**) amygdala and (**d**) cortex. Representative images are shown following staining of 4 mice per group. Data are mean ± s.e.m; *p < 0.05; **p < 0.01; ****p < 0.0001. ANOVA followed by Tukey's post-hoc multiple comparison test. Scale bar: 50µm**.**

References

Boye SL, Bennett A, Scalabrino ML, McCullough KT, Van Vliet K, Choudhury S, *et al.* Impact of heparan sulfate binding on transduction of retina by recombinant adeno-associated virus vectors. J Virol. 2016;90(8):4215-31.

Fagone P, Wright JF, Nathwani AC, Nienhuis AW, Davidoff AM, Gray JT. Systemic errors in quantitative polymerase chain reaction titration of self-complementary adeno-associated viral vectors and improved alternative methods. Hum Gene Ther Methods. 2012;23(1):1-7.

Grimm D, Kern A, Rittner K, Kleinschmidt JA. Novel tools for production and purification of recombinant adeno-associated virus vectors. Hum Gene Ther. 1998;9(18):2745-60.

Kohlbrenner E, Henckaerts E, Rapti K, Gordon RE, Linden RM, Hajjar RJ, *et al.* Quantification of AAV particle titers by infrared fluorescence scanning of coomassie-stained sodium dodecyl sulfate-polyacrylamide gels. Hum Gene Ther Methods. 2012;23(3):198-203.

Rayaprolu V, Kruse S, Kant R, Movahed N, Brooke D, Bothner B. Fluorometric Estimation of Viral Thermal Stability. Bio-protocol. 2014;4(15):e1199.

Rayaprolu V, Kruse S, Kant R, Venkatakrishnan B, Movahed N, Brooke D, *et al.* Comparative analysis of adeno-associated virus capsid stability and dynamics. J Virol. 2013;87(24):13150-60.

Zeltner N, Kohlbrenner E, Clément N, Weber T, Linden RM. Near-perfect infectivity of wild-type AAV as benchmark for infectivity of recombinant AAV vectors. Gene Ther. 2010;17(7):872-79.

Zolotukhin S, Potter M, Zolotukhin I, Sakai Y, Loiler S, Fraites TJ, *et al.* Production and purification of serotype 1, 2, and 5 recombinant adeno-associated viral vectors. Methods. 2002;28(2):158-67.

Supplementary Figure 1. Differential Scanning fluorimetry shows increased thermal stability of AAV-TT.

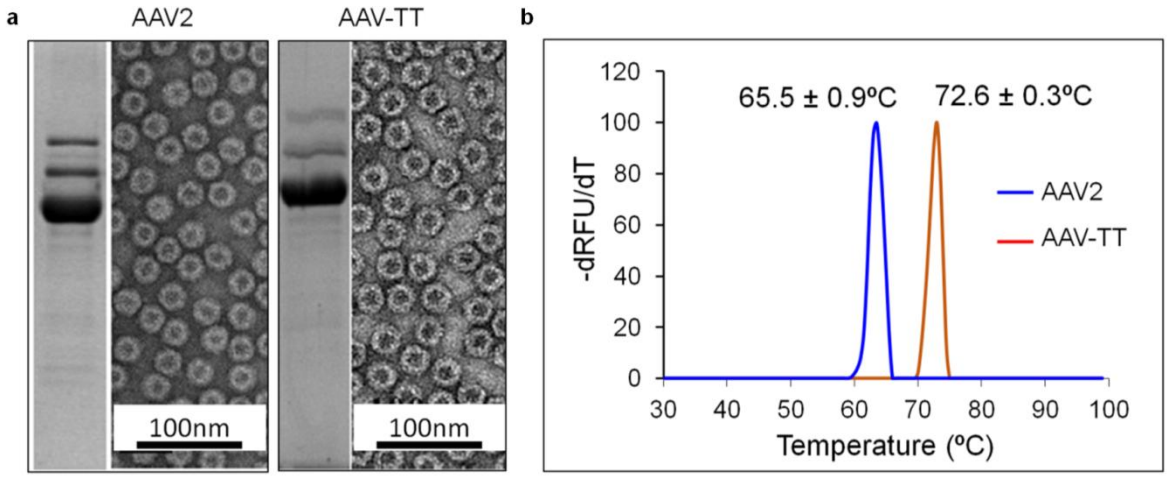

Supplementary Figure 2. AAV-TT exhibits reduced in vitro transduction efficiency and lacks heparin-binding ability.

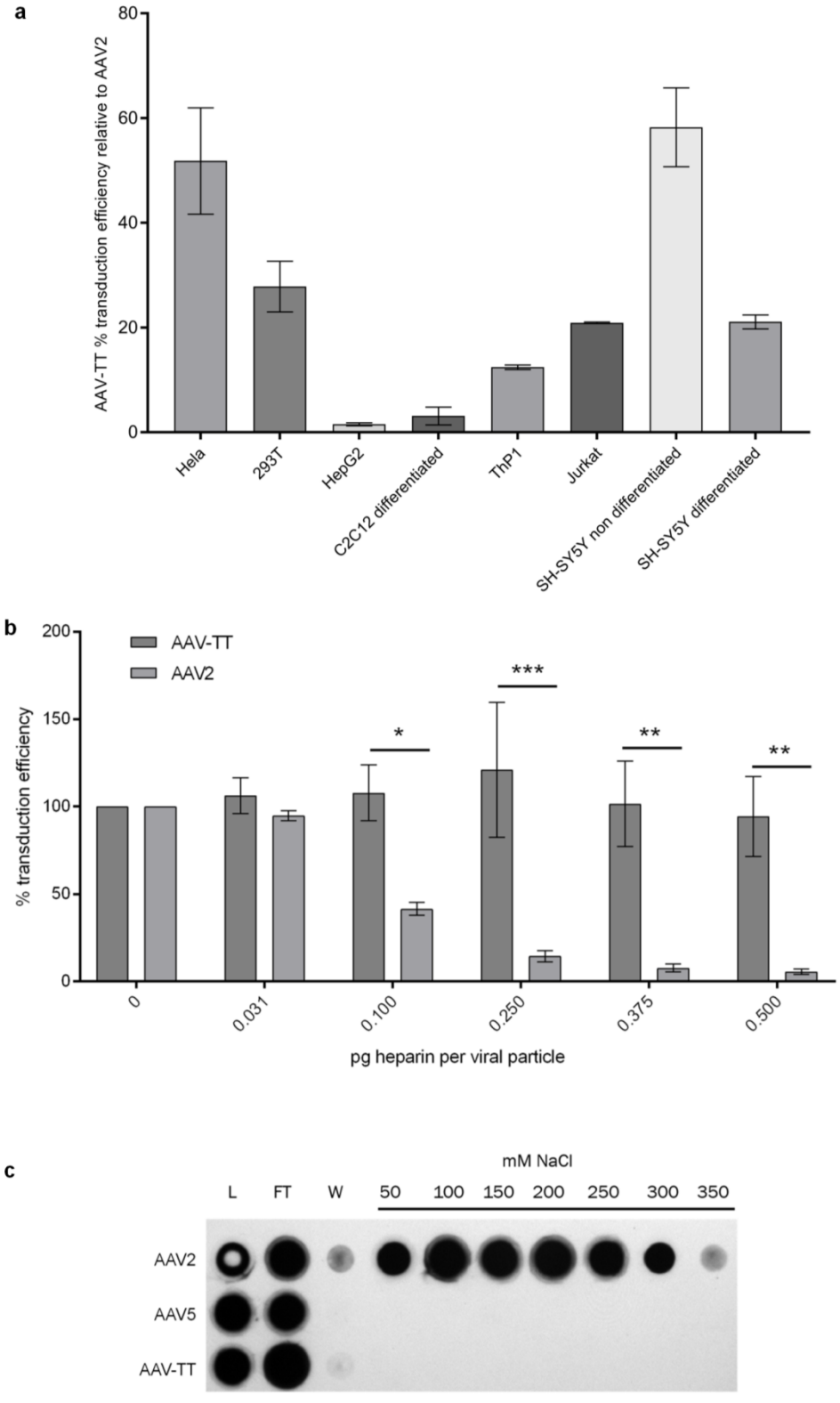

Supplementary Figure 3. Nigral injections in adult rats show superior transduction ability and vector spread.

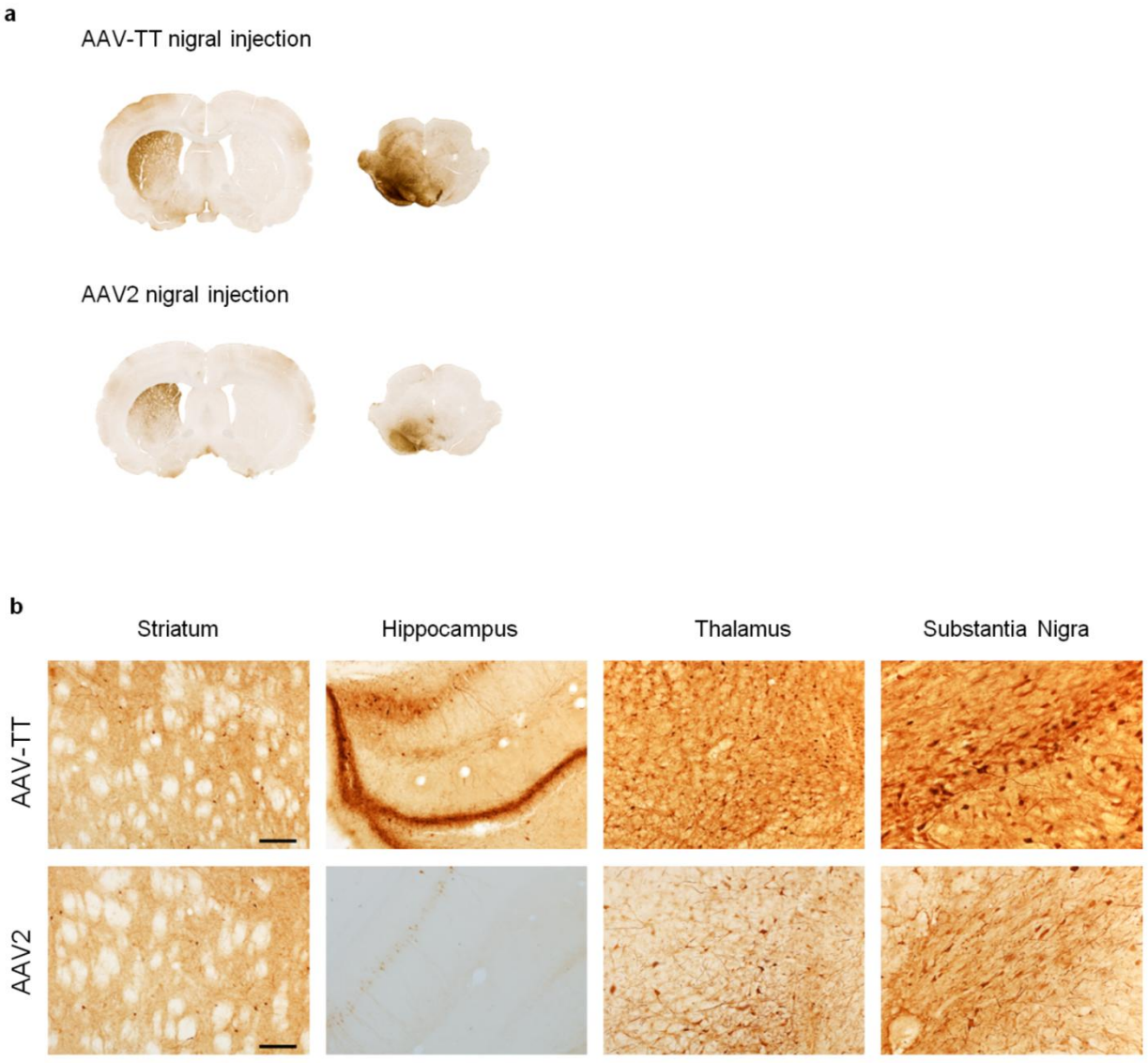

Supplementary Figure 4. Absence of GFP expression in GFAP+ astrocytes and Iba1+ microglia/macrophages in AAV-TT-treated adult mice.

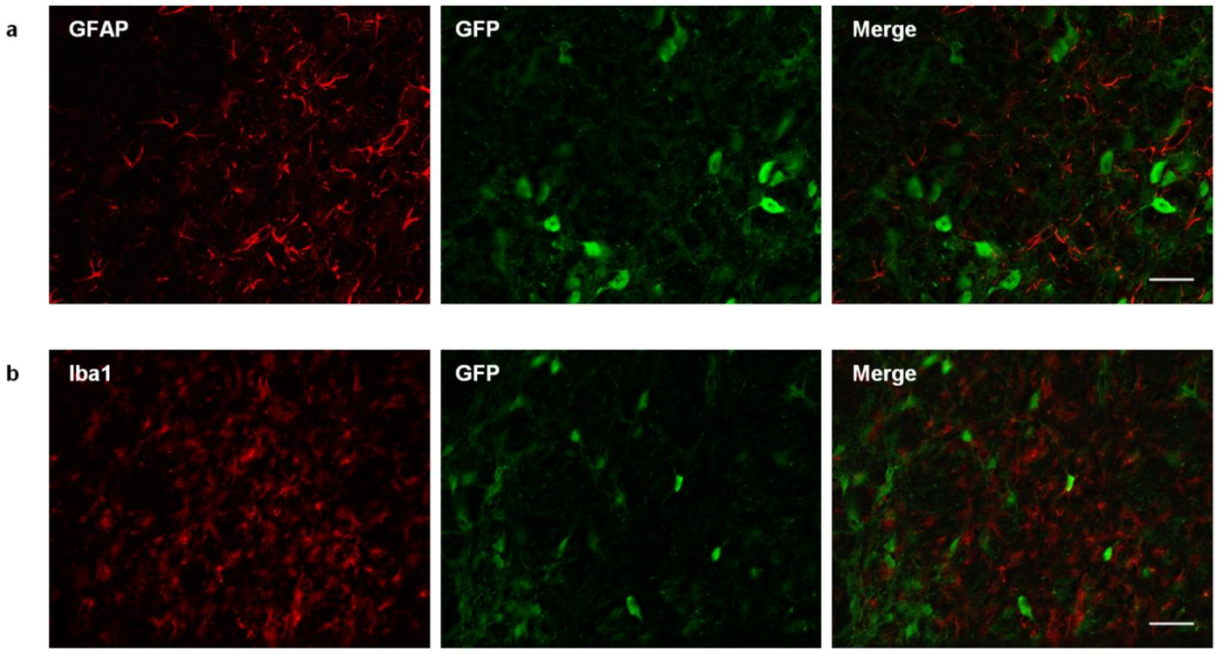

Supplementary Figure 5. Determination of HGSNAT activity *in vitro* and *in vivo* after short-term treatment.

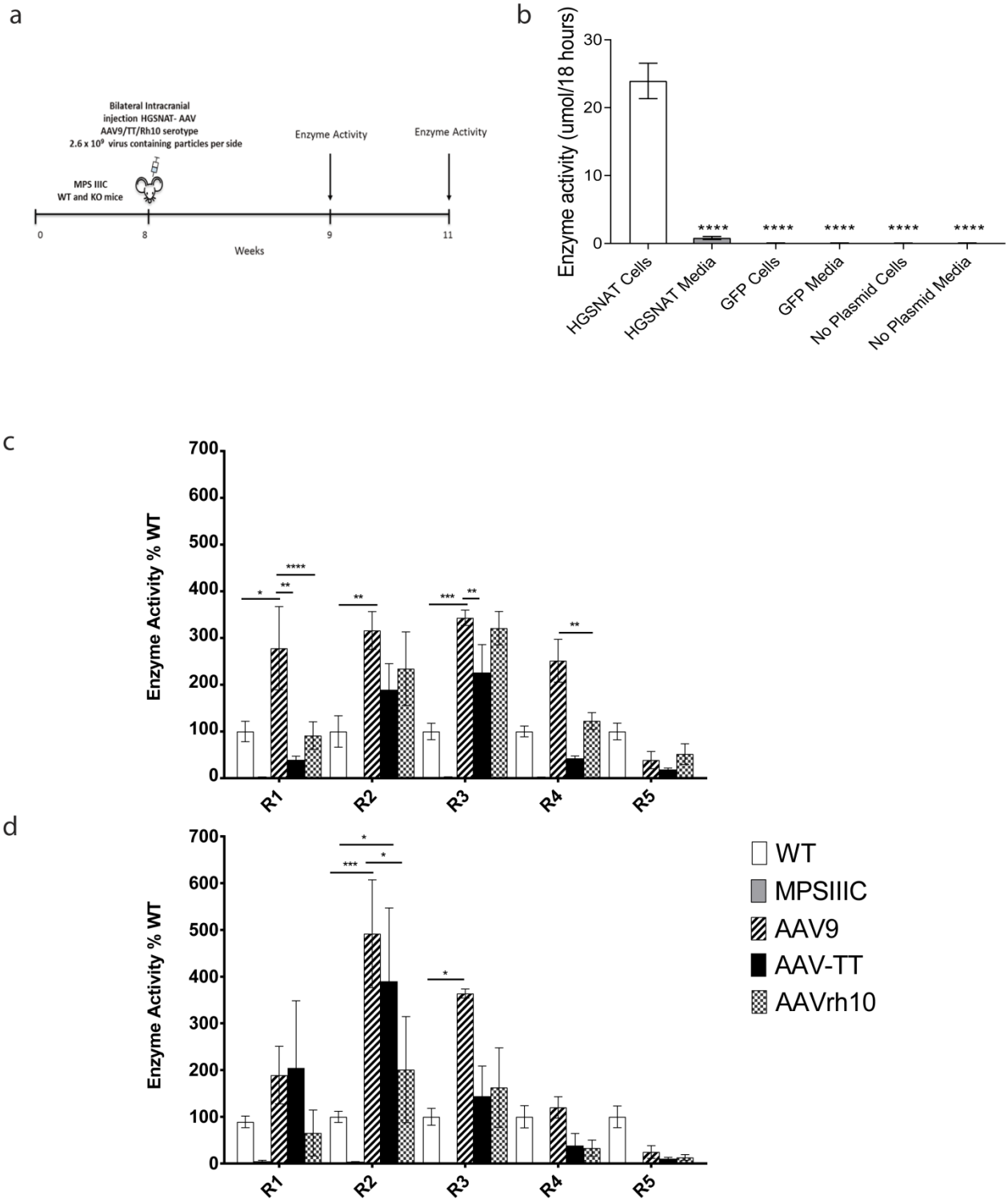

Supplementary Figure 6. Little to no off-target transduction of AAV-TT in peripheral organs.

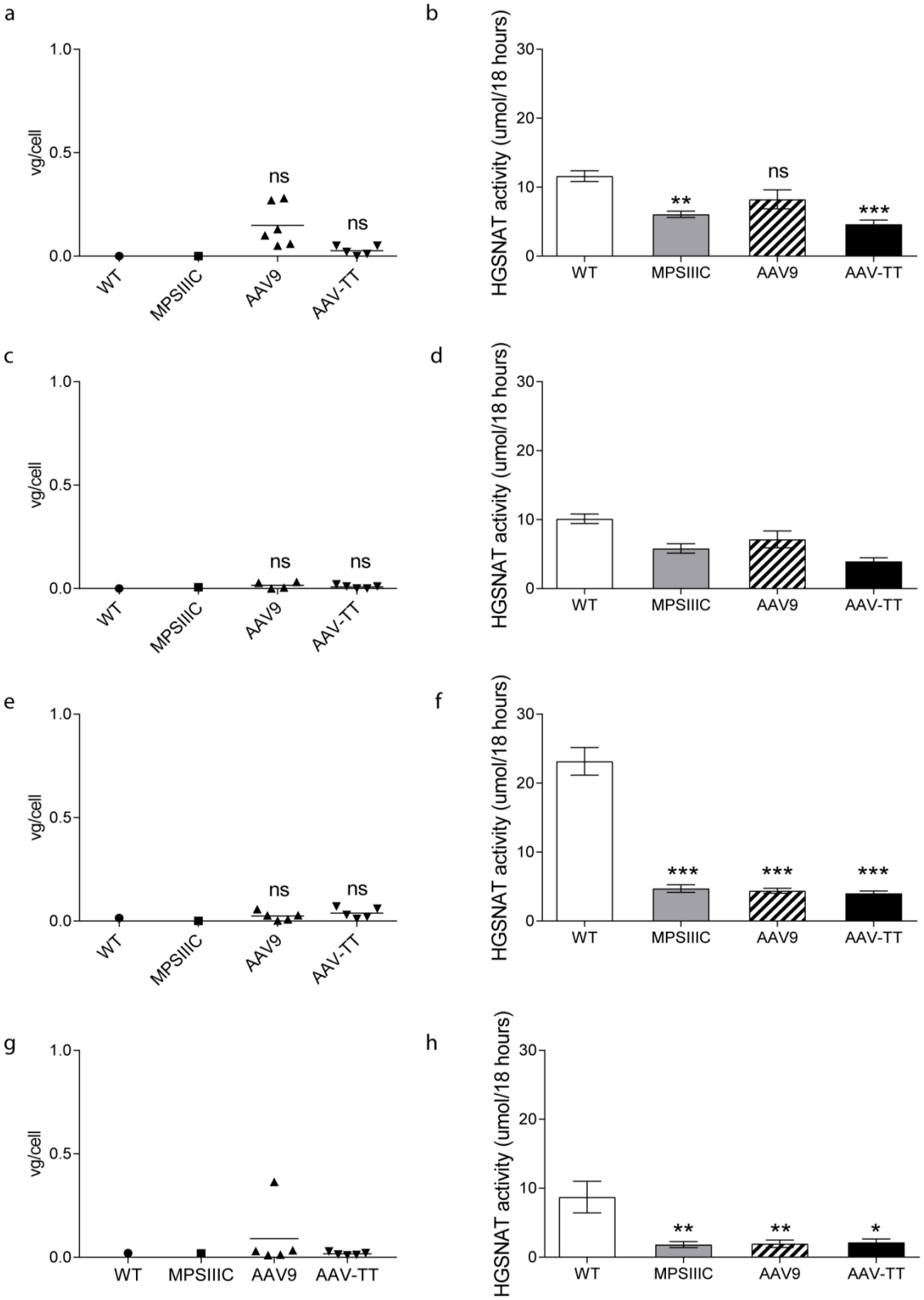

Supplementary Figure 7. AAV-TT and AAV9 correct secondary storage of GM2 and GM3 gangliosides in specific brain regions.

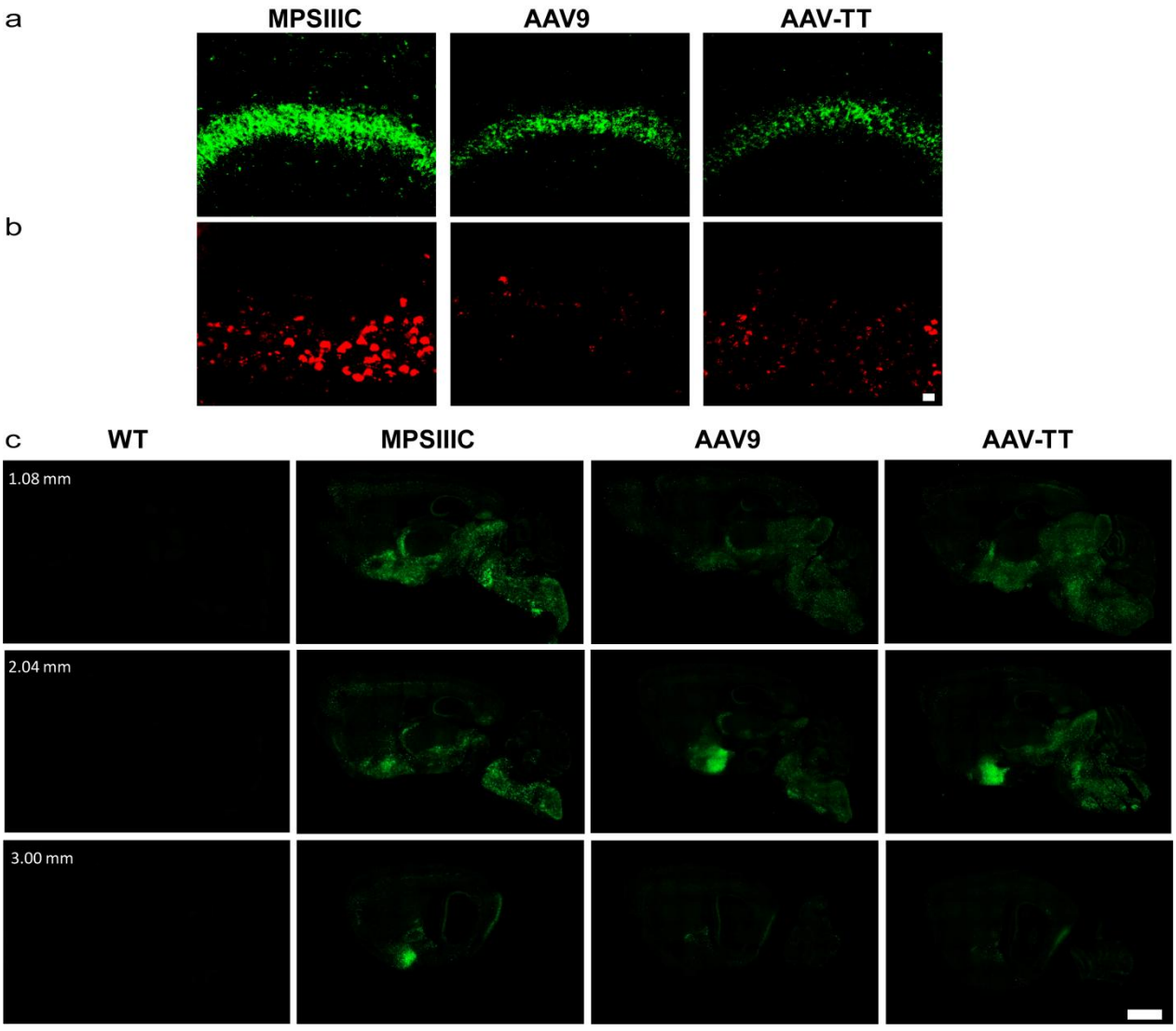

Supplementary Figure 8. AAV-TT and AAV9 reduce astrocytosis. Quantification of GFAP

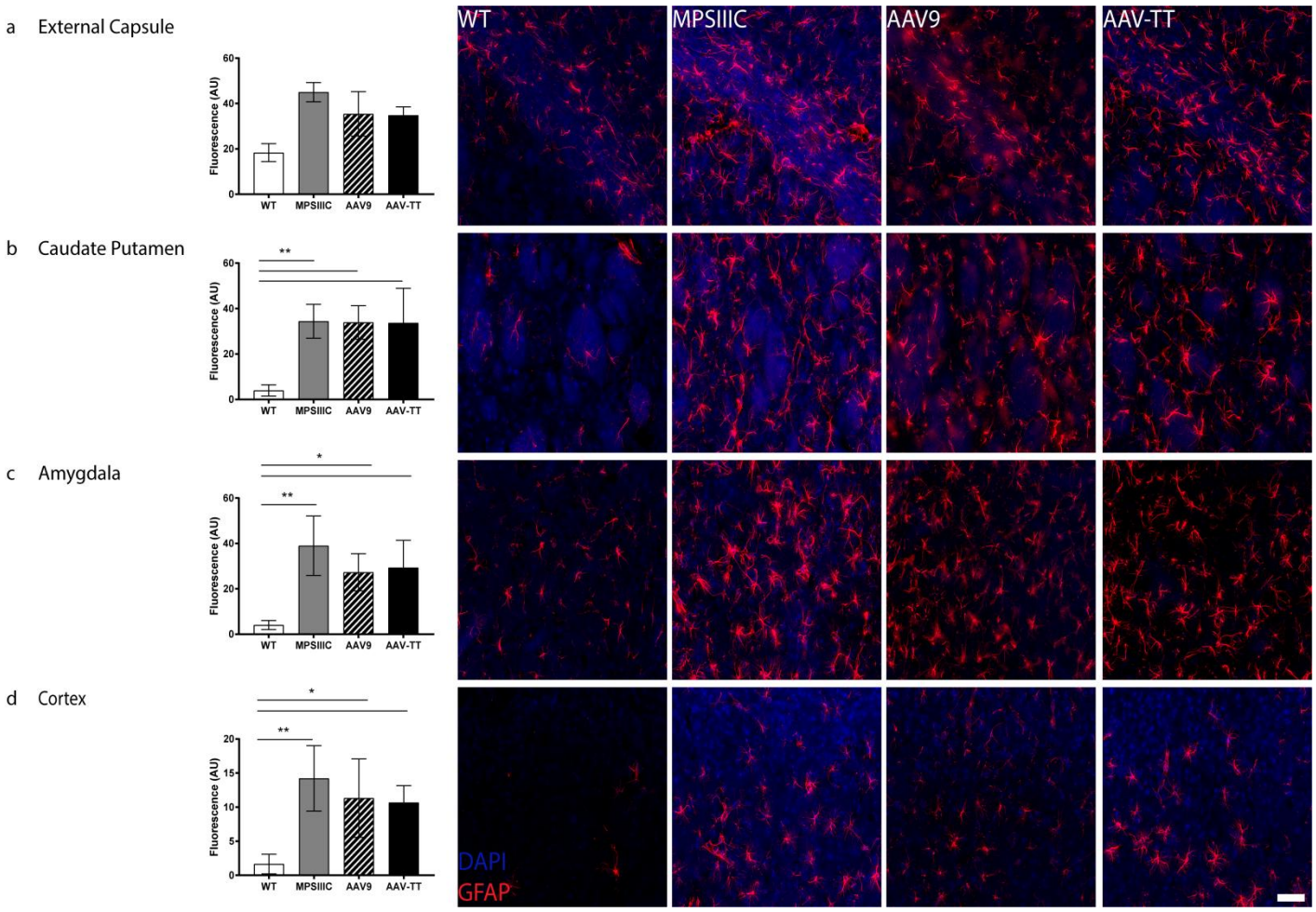

Supplementary Figure 9. AAV-TT and AAV9 reduce LAMP2 lysososmal burden.

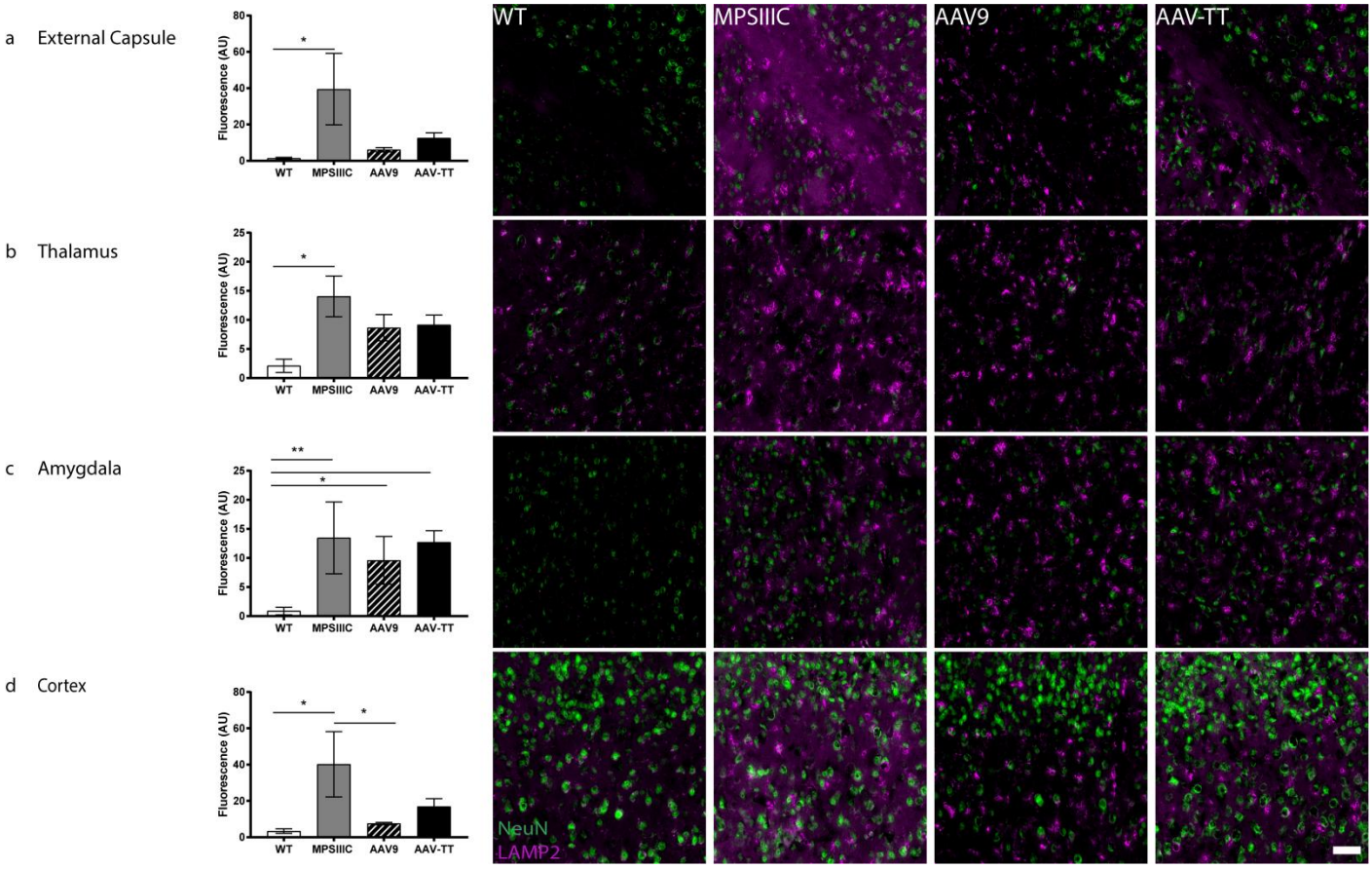

Supplementary Figure 10. AAV-TT corrects neuroinflammation over AAV9. Quantification